AGU ADVANCING EARTH AND SPACE SCIENCE

Earth and Space Science

RESEARCH LETTER
10.1029/2020EA001167

Swarm Observations of Dawn/Dusk Asymmetries Between Pedersen Conductance in Upward and Downward Field-Aligned Current Regions

L. Olifer[1], C. Feltman[2], R. Ghaffari[3], S. Henderson[2], D. Huyghebaert[4], J. Burchill[3], A. N. Jaynes[2], D. Knudsen[3], K. McWilliams[4], J. I. Moen[5,6], A. Spicher[5], and J. Wu[3]

[1]Department of Physics, University of Alberta, Edmonton, AB, Canada, [2]Department of Physics and Astronomy, University of Iowa, Iowa City, IA, USA, [3]Department of Physics and Astronomy, University of Calgary, Calgary, AB, Canada, [4]Physics and Engineering Physics Department, University of Saskatchewan, Saskatoon, SK, Canada, [5]Department of Physics, University of Oslo, Oslo, Norway, [6]The University Center in Svalbard, Longyearbyen, Norway

Abstract The locations of region 1 and 2 field-aligned current systems were determined using fluxgate magnetometer measurements from 875 dawn-dusk passes of the Swarm A satellite. Within each field-aligned current region, the ionospheric Pedersen conductance was derived from the newly corrected Swarm electric and magnetic field measurements. The Pedersen conductances are generally consistent with photoionization models. However, we show that the in situ method of determining Pedersen conductance allows for a more complete description of magnetosphere-ionosphere coupling and should be used in future studies when possible. We show that, overall, the Pedersen conductance is larger in the upward current region than in the downward region by ~0.6 S on the dawn side of the Earth. Meanwhile, the dusk side Pedersen conductance is equivalent in both current regions. We attribute this asymmetry to dawn side energetic electron precipitation, commonly associated with substorm electron injections from the magnetotail.

Key Points:

- In situ Pedersen conductance in field-aligned current (FAC) regions are obtained from the Swarm measurements of the magnetic field and plasma flow velocity
- Pedersen conductance is larger in the upward than downward FAC regions on the dawn side, the dusk side values are similar in both regions
- Asymmetry between dawn and dusk current regions is attributed to intense electron precipitation commonly associated with substorm injections

Supporting Information:

Supporting Information may be found in the online version of this article.

Correspondence to:

L. Olifer,
olifer@ualberta.ca

Citation:

Olifer, L., Feltman, C., Ghaffari, R., Henderson, S., Huyghebaert, D., Burchill, J., et al. (2021). Swarm observations of dawn/dusk asymmetries between Pedersen conductance in upward and downward field-aligned current regions. *Earth and Space Science*, *8*, e2020EA001167. https://doi.org/10.1029/2020EA001167

Received 3 MAR 2020
Accepted 12 JUN 2021

1. Introduction

The coupling of the Earth's magnetosphere and ionosphere via vast current sheets has been investigated using data from satellite missions over the past 40 years. In situ measurements of current intensity from magnetic field deflections (Fujii et al., 1981; Iijima & Potemra, 1976), electron density (Fremouw et al., 1985; Rich et al., 1985), ionospheric conductivity (Fujii & Iijima, 1987; Sugiura et al., 1982), charged particle flux (Rich et al., 1985), ionospheric convection (Burch et al., 1985), and current sheet location (Wang et al., 2005) in the auroral zone have shown various dynamic properties of these current sheets. Magnetic field-aligned currents (FACs), or Birkeland currents (Birkeland, 1913) as they are also known, consist primarily of paired current sheets flowing into and out of the ionosphere in concentric rings at auroral zone latitudes. Near dawn and dusk, there are usually two clear current sheets extended in local time that are adjacent in latitude and flowing in opposite directions, that is, flowing into or out of the ionosphere (Fujii et al., 1981). Iijima and Potemra (1976) described these FAC sheets as two rings of current around 70° magnetic latitude and separated into the region 1 (R1) FAC at higher latitudes and the region 2 (R2) FAC at lower latitudes that overlap in the pre-midnight region. In both the northern and southern hemispheres, the R1 FAC flows downward towards the Earth on the dawn side and upward away from the Earth on the dusk side. In contrast, the R2 FAC flows upward away from the Earth in the dawn sector and downward towards the Earth in the dusk sector. In the ionosphere the R1 and R2 FACs close in part via the ionospheric Pedersen current where the height integrated Pedersen conductivity, Pedersen conductance, Σ_P, allows current to flow between the FAC sheets (Fujii & Iijima, 1987; Haraguchi et al., 2004). The Pedersen conductance can limit the current flow in the ionosphere, regulating the rate at which energy is exchanged between the magnetosphere and ionosphere. For these reasons, Σ_P is an important parameter in understanding magnetosphere-ionosphere coupling and in describing the current flow in the high altitude ionosphere. It is responsible for regulating such processes as ionospheric Joule heating (Palmroth et al., 2005), FAC generation mechanisms (Lysak, 1985), and hemispherical current asymmetries (Greenwald et al., 2002; Lyatsky et al., 2014).

Established methods to derive or model Σ_P have relied on the solar-zenith angle (e.g., Vickrey et al., 1981), particle precipitation (e.g., McGranaghan et al., 2015; Robinson et al., 1987), or the proportionality between low-frequency electric and magnetic field components (e.g., Knudsen et al., 1990; Pakhotin et al., 2018; Sugiura et al., 1982). However, the conductance values derived using these models have not been applied to a comparison study in regions of upward and downward FACs. It is foreseeable that Σ_P may differ in the ionospheric footprint of R1 and R2 FACs due to differences in energetic particle precipitation in the upward and downward FAC regions (Korth et al., 2014; Vickrey et al., 1981). This warrants investigation.

We utilize data from the Swarm mission (Friis-Christensen et al., 2008) in situ electric and magnetic fields instruments measured in 2016 and 2017 to calculate Σ_P in the R1 and R2 FAC sheets. To estimate Σ_P from Swarm data, we apply the linear relation between the electric and magnetic field components described in the next section (cf. Sugiura et al., 1982). A comparison between Σ_P calculated using Swarm data and Σ_P derived from empirical models (parametrized by solar zenith angle) is performed. Using the Swarm Σ_P values, we conduct a statistical analysis of Pedersen conductance in the R1 and R2 FAC sheets for dawn and dusk Swarm satellite passes in both northern and southern hemispheres. A description of the technique used to determine the location of the R1 and R2 FAC sheets is provided in the next section, along with a description of the data used. Differences between Σ_P in the R1 and R2 FACs are examined and possible reasons for the differences are discussed. Finally, we make a case for the importance of electron precipitation on Σ_P at E-region altitudes. The novelty of this study is that we take the advantage of the extensive data base of Swarm, as well as previous work by Sugiura et al. (1982) and Knudsen et al. (1990), to compare Σ_P in the large-scale R1 and R2 FAC sheets.

2. Data and Methodology

In this research, we use in situ observations of the magnetic and electric fields by the Swarm A satellite (Friis-Christensen et al., 2008) to derive Σ_P values. The spacecraft has a near-polar low-Earth orbit with an altitude of ~460 km and an orbital period of ~1.5 h. The electric field at Swarm A is derived from measurements of the cross-track ion drift velocity at 2 Hz from the electric field instrument (EFI) (Knudsen et al., 2017). In a validation study of the cross-track ion drift data, Lomidze et al. (2019) developed an improved calibration scheme, which has been adopted as the basis of a new data set (version 0301) officially released by ESA in July 2020 on the ESA web site. We also use the magnetic field data from the vector fluxgate magnetometer (Friis-Christensen et al., 2008). These data are down-sampled from 50 to 2 Hz to match the EFI resolution. A combination of the ion drift velocity, $\mathbf{v}_i$, and the magnetic field measurements, $\mathbf{B}$, are used to calculate the electric field vector, $\mathbf{E}$, making use of the generalized Ohm's law for frozen-in plasma: $\mathbf{E} = -\mathbf{v}_i \times \mathbf{B}$. The quality of the Swarm EFI electric field data has been assessed through comparison with the ground-based observations and empirical models (e.g., Koustov et al., 2019; Lomidze et al., 2019). The magnetic and electric fields are provided in the spacecraft coordinate system, with the x-axis pointing along the trajectory of a satellite, the y-axis pointing horizontally and to the right from the perspective of the satellite track, and the z-axis completing the right-handed coordinate system.

Within FACs in the topside ionosphere, the ratio of quasi-static electric and magnetic perturbations E_x and δB_y is equal to $(\mu_0 \Sigma_P)^{-1}$ under the assumption of infinite sheet currents that close through regions of height-integrated Pedersen conductance (Sugiura et al., 1982). In this approximation, E_x is normal to the sheet, and Hall currents flow along the lower boundary of the sheet and are divergence-free, and therefore do not contribute to FACs. Variations in Hall conductivity across the sheet coupled with a tangential component of the electric field would lead to additional FACs and are a potential source of error in this simple model, as are non-planar current structures. The quasi-static approximation breaks down for variations faster than ~10 s (Knudsen et al., 1992).

Figure 1 shows the along-track electric field component, E_x, in the top left panel and the perturbation of the cross-track magnetic field component, δB_y in the bottom left panel measured during one auroral zone crossing by Swarm A. The perturbed magnetic field δB_y component is calculated by subtracting the unperturbed magnetic field component, as provided by the International Geomagnetic Reference Field (IGRF-2015) model (Thébault et al., 2015), from B_y measured by the Swarm magnetometers.

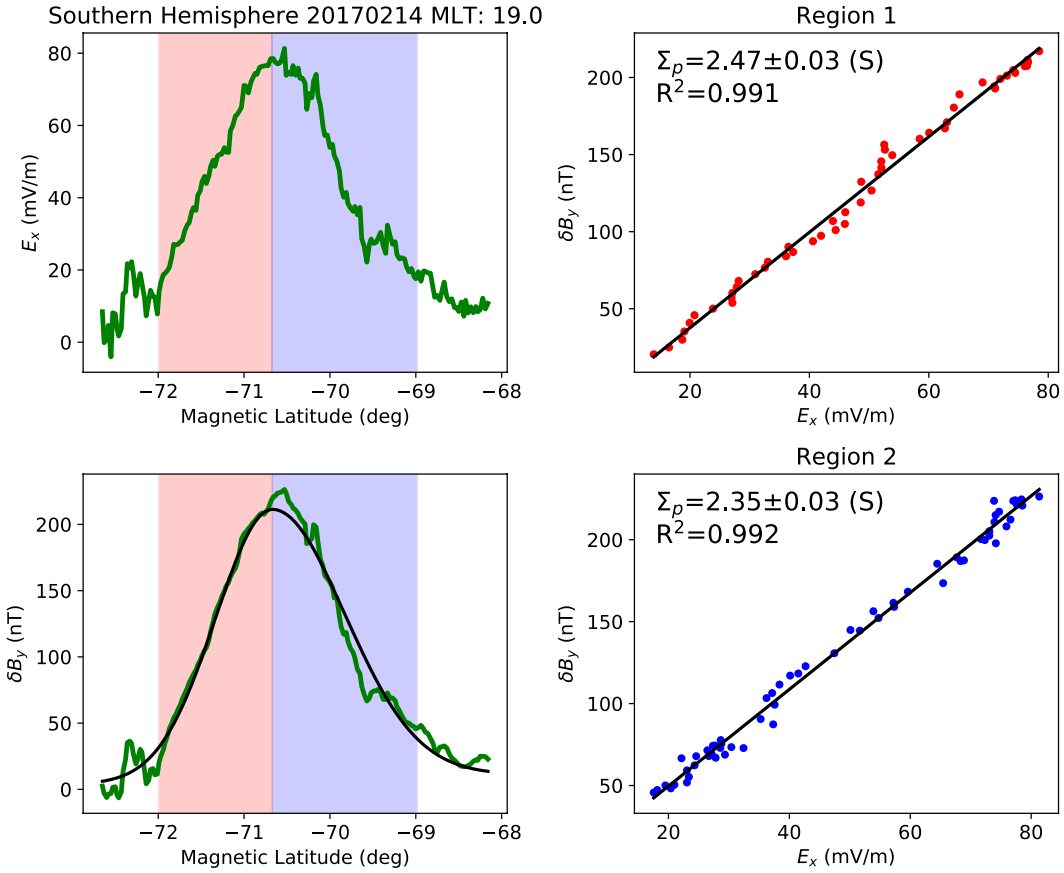

Figure 1. Example of single-pass measurements from Swarm A on February 14, 2017 at 19 MLT. The upper left panel shows the measured electric field in green with region 1 (R1) and region 2 (R2) field-aligned currents (FACs) indicated in red and blue, respectively. Color indicates the direction of the current in each region; red represents upward and blue downward currents. The lower left panel shows measured δB_y in green with a double-sided Gaussian fit in black. The upper and lower right panels show the correlation of the δB_y and E_x measurements for R1 and R2 FAC sheets, respectively. The FAC regions are fitted separately to produce separate Σ_P. The best-fit Σ_P values, along with the R^2 correlation coefficients, are shown in the top left corner of the panels.

In this study, we take a novel approach of determining the extent of the R1 and R2 FACs using a non-linear least squares double-sided Gaussian fit to the δB_y measurements. The fitted double-sided Gaussian function is defined as follows:

$$\delta B_y(\phi) = \begin{cases} (A - b_1)\exp\left\{-\dfrac{(\phi-\mu)^2}{2\sigma_1^2}\right\} + b_1, & \text{if } \phi < \mu \\ (A - b_2)\exp\left\{-\dfrac{(\phi-\mu)^2}{2\sigma_2^2}\right\} + b_2, & \text{otherwise,} \end{cases} \quad (1)$$

where ϕ is the magnetic latitude, μ defines the latitude of the boundary that separates R1 and R2 FAC regions, and A, b_1, b_2, σ_1 and σ_2 are Gaussian fit parameters. The width of the FAC sheets is defined as twice the standard deviation of the Gaussian fit, that is, a $2\sigma_1$ or $2\sigma_2$ distance from the peak of the fitted half-distribution. The 2σ FAC width ensures that the highest current density flowing in the determined region is located in the middle. The FACs are denoted by R1 and R2 in the figure. Light red shading indicates an upward current, and light blue shading indicates a downward current.

Figure 1 also includes a demonstration of the technique used to calculate Σ_P values in the R1 and R2 FAC crossings from in situ Swarm electric and magnetic field data. The data used to calculate the R1 Σ_P value

are presented in the top right panel, and those for the R2 Σ_P value in the bottom right panel. Similar to previous studies (e.g., Knudsen et al., 1990; Pakhotin et al., 2018; Sugiura et al., 1982), we calculate Σ_P from a linear fit to the equation $\delta B_y = \Sigma_P \mu_0 E_x$, where μ_0 is the magnetic permeability of free space. The best-fit lines, which represent the Σ_P value across the FAC region, are plotted in the right-hand panels of Figure 1. Note that this approach of determining the conductance assumes that the Swarm satellites pass approximately perpendicularly through a quasi-static FAC sheet. However, for crossing angles θ less than 90° the error is negligible, since the Swarm cross-track measurements of ion drift and magnetic perturbation represent the values tangential to the FAC sheet multiplied by $\cos(\theta)$, however the ratio $E_x/\delta B_y$ is unaffected. The correlation coefficient R^2 between δB_y and E_x represents the goodness of the linear least squares fit. The R^2 values are listed in the right-hand panels. Notably, the uncertainty in the electric field baseline for a given crossing does not affect the estimated Σ_P values because they are derived from the slope of the B_y-E_x relationship. However, the sensitivity of the EFI instrument can introduce additional uncertainties to the analysis, thus we only use quality electric field data as provided in the EFI ion drift data set.

During the period from January 2016 through May 2017, there were a total of 6,182 auroral zone crossings by Swarm A that contained simultaneous measurements of the magnetic and electric fields. These include passes in both the northern and southern hemispheres. Of these passes, 2,500 auroral zone crossings had a two-FAC structure with a clear delineation between the R1 and R2 FACs, that is, only one double-sided Gaussian was needed to fit the latitudinal δB_y variation. Notably, this fitting approach fails in the regions of more complex magnetic field variations near noon and midnight due to the presence of the Harang discontinuity near midnight (Erickson et al., 1991) and to the presence of the region 0 FACs near noon (Watanabe et al., 1998). The selected passes for this study contain only good fit results as determined by a relative uncertainty of fitting parameters being less than 10%. We additionally confine our analysis to the dawn and dusk sectors. We apply the approach described above for calculating Σ_P to the 1,987 auroral zone crossings. The total number of crossings selected for the analysis is further reduced to 875 passes after excluding those with poor correlation, that is, with R^2 of the linear fit of the δB_y and E_x ratio that are less than 0.5. The final event list of 875 auroral zone crossings are assessed in the statistical analysis presented below. The list of selected events, as well as corresponding Pedersen conductance and directionality of both FAC regions, are presented in the Table S1. The satellite coverage during those events is shown in Figure S1. It is also important to note that the introduced in this paper algorithm of determining the filed aligned currents regions from the Swarm satellite data can be easily expanded to study more complex FAC morphology in the midnight and noon local time regions. While not assessed in this work, this method can serve as a starting point for such studies in the future. Notably, the approach used in this paper for analyzing properties of field-aligned current regions using the Swarm satellite data can be easily expanded for future studies of more complex FAC systems in the noon and midnight sectors.

In addition to the Swarm A observational data, we have analyzed the solar wind conditions and the geomagnetic activity during the selected events utilizing data from the OMNI database (King & Papitashvili, 2005). The results, provided in the Figure S2, show that the events selected in this study predominantly occurred during quiet conditions. For instance, the auroral electrojet (AE) index during 78% of the events in this study is below 300 nT. This is expected for the 2016–2017 period under investigation, as it is a solar minimum period.

3. Results

We compare the Σ_P values calculated using in situ Swarm A data with modeled values of Σ_P that are functions of solar zenith angle χ and of a proxy for quiet time extreme ultraviolet (EUV) solar flux. Two representative models of photoconductance were considered for comparison with the derived values of Σ_P from Swarm. The photoconductance model of Vickrey et al. (1981) was derived using Chatanika incoherent scatter radar data and resulted in the relatively simple relation: $\Sigma_P = 5\sqrt{\cos\chi}$ for $\chi \leq 87°$. This model did not include a factor to account for the variation of solar EUV flux through the solar cycle. The photoconductance model of Moen and Brekke (1993) accounts for variability of plasma production by solar EUV through the solar cycle by using the solar radio flux at 10.7 cm as a proxy for solar EUV flux. The Σ_P model proposed by

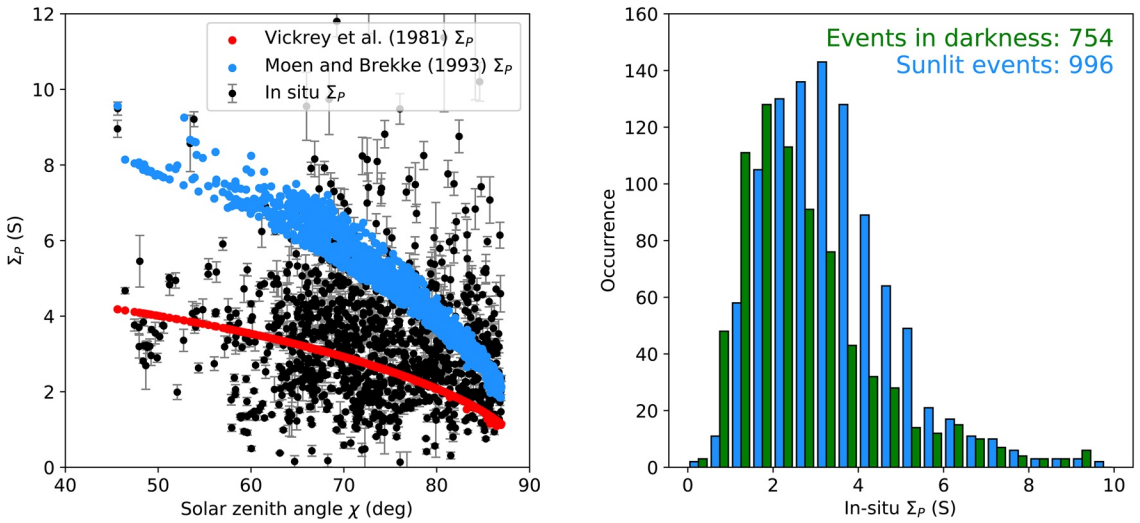

Figure 2. A comparison of the in situ derived Σ_P values with those obtained from the Vickrey et al. (1981) and Moen and Brekke (1993) models. The left panel shows in black a scatter plot of the calculated average Σ_P values from the Swarm measurements as a function of the average solar zenith angle per satellite pass. Only the sunlit events are included in the left-hand panel. Modeled Σ_P values for the sunlit Swarm events from the Vickrey et al. (1981) model are in red, and from the Moen and Brekke (1993) model in blue. The error bars of the Swarm Σ_P values were obtained from the fitting procedure described above. The right-hand panel is a comparison of the distributions of in situ Swarm Σ_P events during sunlit and dark conditions in blue and green, respectively.

Moen and Brekke (1993) has the form $\Sigma_P = S^{0.49}(0.34\cos\chi + 0.93(\cos\chi)^{0.5})$, where S is the solar flux (F10.7) index and χ the solar zenith angle. The daily F10.7 cm flux values were obtained from the OMNI database.

For our study, values of χ were determined for all data points along a satellite crossing through a R1 or R2 FAC sheet. These χ values were used to calculate modeled Σ_P values for all points in the pass through the FAC sheet. For each FAC sheet, both the χ values and the model Σ_P values were averaged. The averaged values of χ and Σ_P are presented in Figure 2. We compare the averaged modeled Σ_P values with the in situ Swarm Σ_P values derived using the linear least-square fitting method described above.

The left panel in Figure 2 includes the Σ_P values derived from the in situ Swarm observations, as well as those from the two photoionization models. For comparison purposes, only the data-derived points where a modeled Σ_P was possible to calculate are included. Points on the nightside, that is, where $\chi > 87°$, are excluded. The in situ Swarm Σ_P values are represented by the black dots, and the associated error bars represent the one-sigma standard deviation from the linear least squares fits. The model values from Vickrey et al. (1981) are represented by the red dots, while those from Moen and Brekke (1993) are represented by blue dots. The in situ Σ_P values fall mostly above the model proposed by Vickrey et al. (1981). However, the Pedersen conductance from Moen and Brekke (1993) model is consistently larger than both in situ and Vickrey et al. (1981) data. The variability of the in situ Swarm Pedersen conductance values as a function of the solar zenith angle is much higher than that predicted by the photoionization models, and is likely due to the high variability of the E-region electron density resulting from auroral precipitation. This result shows that heuristic photoionization Pedersen conductance models do a poor job of predicting Σ_P values inside FAC regions. We suggest that further validation of the Swarm-based Σ_P values by comparing with those calculated from directly measured density profiles using incoherent scatter radar techniques are needed. Other systematic effects should be considered, for example, the fact that E and B fields varying on time scale from 0.1 to 1 s will form a standing wave pattern which will modify the E/B ratio above the reflection altitude (Knudsen et al., 1992), or the effect of non-planar FAC structures. Such analyses can potentially shed some light on lower in situ Σ_P values found here in comparison with Moen and Brekke (1993) model. It is important to note that, in addition to photoconductivity, the Swarm Σ_P values can also include conductivity contributions from other processes, such as particle precipitation and plasma transport.

The right panel of Figure 2 contains two distributions of Σ_P values, obtained in sunlit and dark conditions, corresponding to $\chi \leq 87°$ and $\chi > 87°$, respectively. Notably, a large fraction of the Swarm events fall in "dark" regions where the solar zenith angle models are not applicable. Figure 2 shows that the distribution

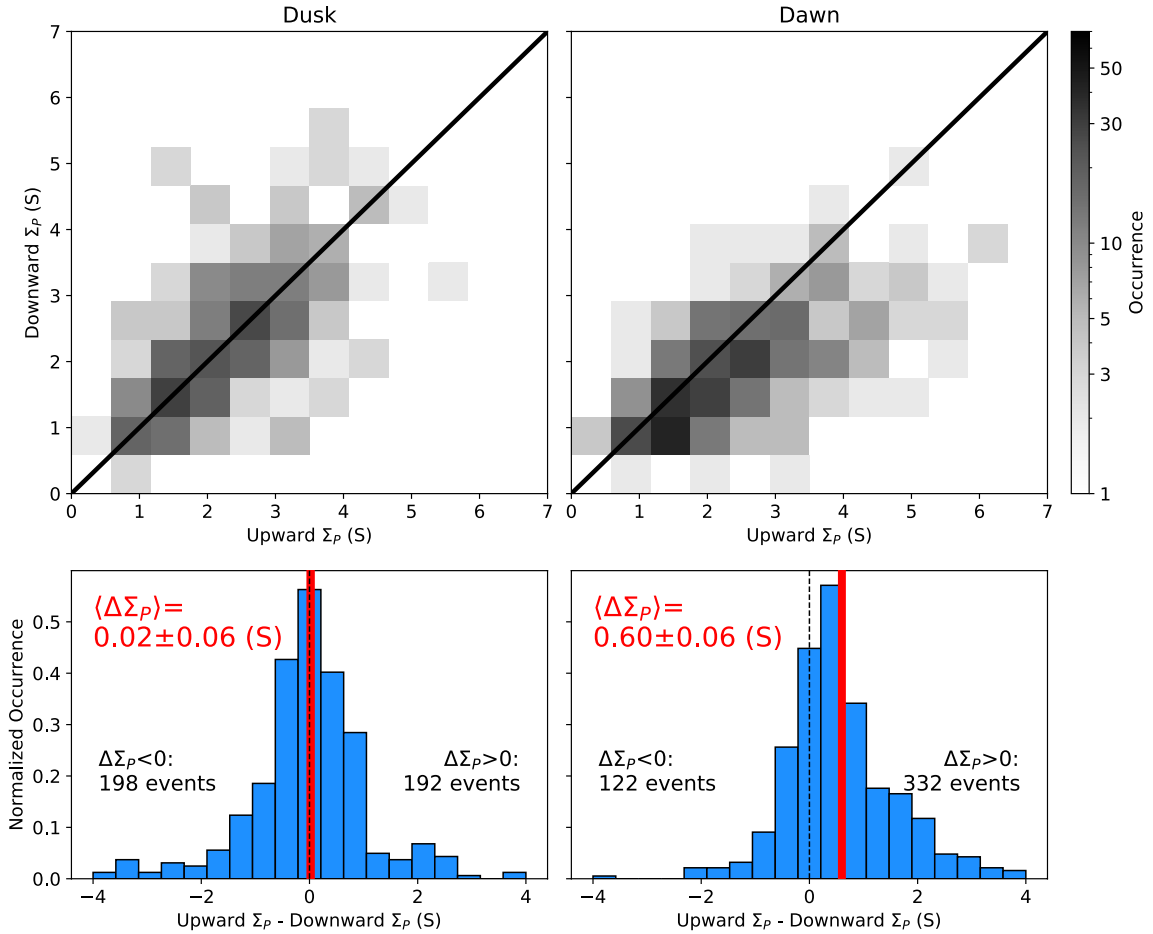

Figure 3. Comparison of the Σ_P values in the upward and downward field-aligned current (FAC) regions in the dusk (left column) and dawn (right column) sectors. The top row contains two-dimensional occurrence histograms of the values of Σ_P in the upward and downward neighboring FAC regions. The solid diagonal lines in the upper panels represent the unity ratio of Σ_P in neighboring FAC regions. The bottom row shows the distribution of differences between upward and downward Σ_P. The vertical red line represents the mean value of the difference $\Delta\Sigma_P$, and its thickness corresponds to the standard deviation of the mean. The mean and the error values are included as red text in the bottom panels. The vertical dashed lines represent value $\Delta\Sigma_P = 0$.

of Swarm Σ_P values measured during "dark" conditions are lower than those derived from passes through a sunlit ionosphere. Note that empirical Pedersen conductance models, driven by the solar zenith angle, assume a constant and relatively small (~1 S) value of Σ_P in dark conditions. Nonetheless, the right panel of Figure 2 shows that the typical Σ_P values in both sunlit and dark conditions range up to ~6 S. This confirms that an empirical Σ_P model based on the solar zenith angle is unable to accurately represent the data when in darkness. For this reason, the in situ method of determining Σ_P used in this study allows for a more thorough examination of ionosphere conductance.

Determining Σ_P from the in situ measurements separately in the R1 and R2 FAC sheets allows for the study of processes that are active in the different FAC regions. For example, regions of upward FAC are expected to have higher conductance than regions of downward FAC due to electron precipitation into the atmosphere in the upward FAC band. Figure 3 is a comparison of the Σ_P values in adjacent R1 and R2 FAC sheets in the dawn and dusk sectors. In contrast to previous studies, rather than being sorted by FAC region, they are sorted by their direction into or out of the ionosphere. The top row of Figure 3 includes the occurrence diagrams of Σ_P values in downward versus upward adjacent FAC sheets during a Swarm pass. That is to say, each point in the occurrence distribution represents the ratio of Σ_P in adjacent R1 and R2 FAC sheets during one satellite crossing of the auroral oval. In the dusk sector, the distribution of this ratio lies relatively closely to the unity line, indicating little difference between the values of Σ_P in the adjacent upward and downward FAC regions in a Swarm pass across the auroral zone. In the dawn sector the distribution tends

to lie below the unity line, indicating that Σ_P in the upward FAC bands exceeds Σ_P in the adjacent downward FAC bands. To better illustrate the deviation from unity, the differences between the Σ_P values in adjacent FAC regions are presented in the occurrence distributions in the bottom panels of Figure 3.

The occurrence distributions of the difference between the Σ_P values in the adjacent upward and downward FAC regions in the dusk and dawn regions are represented by the histograms in the bottom panels of Figure 3. The mean values of the distributions are represented as red vertical lines. The width of the red lines indicates the error of the mean, which is the standard deviation of the mean of the distribution. The occurrence diagrams, as well the difference distributions, reveal an apparent asymmetry of Σ_P differences in upward and downward FAC regions in the dawn and dusk sectors. The dusk sector (left column of Figure 3) shows a symmetric distribution of Σ_P values in both upward and downward current regions around zero. Notably, the mean difference of Σ_P values in the upward and downward current regions in the dusk sector is zero within one standard error of the mean. This suggests that the electron precipitation expected in the dusk side upward FAC sheet is not sufficient to provide a perceptible difference in Σ_P between the full width of upward and downward FAC regions.

On the other hand, in the dawn sector (right column of Figure 3) there is a consistently larger Σ_P in the upward FAC region (R2). Our analysis shows that, on average, Σ_P in the upward FAC sheet is 0.60 ± 0.06 S larger than in the adjacent downward FAC band. This suggests that precipitation in the dawn sector is likely sufficient to sustain a perceptible increase in ionospheric plasma density over large scales that encapsulate ~3° in latitude.

4. Discussion and Conclusions

The linear least squares fitting method of Sugiura et al. (1982) was used to calculate values of Σ_P in R1 and R2 FAC bands traversed by the Swarm A satellite. The along-track electric field E_x and the perturbation of the cross-track magnetic field δB_y are generally well correlated during an R1 or R2 FAC crossing. In this study we focused on relatively quiet events where two distinct current sheets are present and where the R^2 correlation coefficient between E_x and δB_y is above 0.5 in both adjacent FAC regions. This method, which relies on in situ satellite data, allows Σ_P to be determined within relatively localized regions of interest, in contrast to studies that rely on particle precipitation-based models or solar zenith angle-constrained models.

On average, the Σ_P values derived from in situ Swarm measurements are consistent with correspond to the values derived from two representative conductance models within the same order of magnitude (Moen & Brekke, 1993; Vickrey et al., 1981). In particular, the in situ derived Σ_P values fall in between those predicted by the photoionization models while following the general trend of increasing conductance with decreasing solar zenith angle. Interestingly, the range of the Swarm-derived Σ_P values is closer to those predicted by the Moen and Brekke (1993) model. Nonetheless, neither of the photoionization models capture the level of variability present in the Swarm data. As stated earlier, there are many aspects in the determination of Σ_P that are not taken into account by these models, therefore, it is advantageous to use time-specific Σ_P values which can be derived from radar data or the Swarm satellites, as shown in this study.

Models driven by the solar zenith angle predict $\Sigma_P = 0$ in dark conditions. Hence, the in situ derived values of Σ_P are important for obtaining an accurate depiction of the magnetosphere-ionosphere coupling processes (McGranaghan et al., 2016), as the night-side Pedersen conductance can be finite. This point was also investigated by Moen and Brekke (1993) (their Figure 1) where the event-specific Σ_P values, determined from the ground-based incoherent scatter radar data, on the night side varied between 1 and 10 S. These effects were attributed to particle precipitation and not included in the final Moen and Brekke (1993) model. Nonetheless, nightside Moen and Brekke (1993) Σ_P values are similar to those obtained in this research. Notably, the peak of Σ_P values for dark conditions in our results is shifted to a lower value when compared to the value for the sunlit conditions. The method of deriving Σ_P using the Swarm satellite instrumentation provides a valuable tool for further investigation of physical phenomena occurring in R1 and R2 FACs that can account for the effects of charged particle precipitation.

We have shown that the Σ_P in the R1 and R2 FAC sheets can have substantially different values. The dawn side passes have the largest difference between Σ_P in R1 and R2 FAC sheets. This is evidenced by the upward

FAC Σ_P (R2) being larger than the downward FAC Σ_P (R1) (see the right-hand panels of Figure 3). Upward FACs causing an increase in Σ_P have been previously reported and studied by Marsal (2015), where the increase in conductance is attributed to energetic electron precipitation. The asymmetry in the dawn-dusk conductance has also been reported in the past (Newell et al., 1996), though not separated according to upward and downward FAC directions. Precipitating electrons in the dawn sector can have energies of 1–100 keV (Feldstein et al., 2001; Jaynes et al., 2013; Lyons & Fennell, 1986), which can increase E-region ionization (Fang et al., 2010; Lummerzheim & Lilensten, 1994), and thereby enhance Σ_P. Similar conclusions have been reported by Hardy et al. (1987) where the developed statistical model of Pedersen conductance shows the enhanced Σ_P values equatorward in the dawn region. Notably, Hardy et al. (1987) in their study do not separate into the upward and downward current regions. However, an asymmetry between dawn and dusk regions is evident in the top panel of their Figure 2 where the dawn side Σ_P values are skewed towards the equator, similar to the observations on this paper.

Energetic electron (>1 keV) precipitation in the dawn sector is often associated with electron injections from the magnetotail during substorm breakup (e.g., Akasofu, 1968; Duthie & Scourfield, 1977). The newly injected electron population is scattered into the loss cone through resonant interaction with plasma waves, in particular whistler mode chorus (e.g., Jaynes et al., 2015; Nishimura et al., 2010, 2011; Thorne et al., 2010) and can be a long-lasting, large-scale phenomenon (Jones et al., 2011). Notably, whistler wave generation and electron precipitation happen predominantly in the dawn sector. This is similar to the observations shown in Figure 3 where the effect of the particle precipitation on the ionospheric conductance is apparent only in the dawn sector (see e.g., review by Li et al., 2011). Thus, it is interesting to connect the enhanced Σ_P values with processes responsible for the generation of pulsating auroras. For this purpose, we separate the events into those having low AE index (below 166 nT) and high AE index (above 166 nT). The AE index of 166 nT, used as the boundary between low and high levels of auroral activity, corresponds to the median AE index in the selected events, ensuring approximately the same size of the four datasets. Figure S3 shows the Σ_P difference distributions for those conditions in the dawn and dusk sectors and shows that the largest enhancement of Σ_P values in the upward FAC regions is associated with times of high AE index. This result suggests that the substorm dynamics and night-side injection of the new source population is an important process not only for the radiation belt and inner magnetosphere physics, but also for controlling the extent of the magnetosphere-ionosphere coupling through the field-aligned currents. However, a direct connection between the substorm breakup and enhanced asymmetry of Σ_P values remains to be explored using, for example, conjugate in situ particle measurements from both LEO and highly elliptical orbit missions.

Another potential source of the difference in Σ_P between the dawn side R1 and R2 FACs is plasma transport. For this to be the case, the lower-density plasma would have to be transported to the R1 FAC region and/or denser plasma would have to be transported to the R2 FAC region. This scenario is unlikely due to the typical convection pattern being sunward for R2 FACs and anti-sunward for R1 FACa (Feldstein et al., 2001), which would tend to result in a lower plasma density in R2. In addition to this, the dawn-dusk asymmetry of Σ_P would not be present if the effect were, like the upward and downward FAC sheets, aligned with the two-cell convection pattern, which is typically symmetric in general during moderately quiet geomagnetic conditions as assessed in this paper. In addition, we attribute the variability in the conductance to variability in the E-region electron density where the plasma neutralization time is on the order of seconds. Hence, it is more likely that there is a long-lasting local plasma generation source that results in elevated conductances, for example, as previously discussed, energetic electron precipitation.

Overall, the present study shows the following:

1. The magnetic and electric field measurements by the constellation of Swarm satellites are used to accurately determine the locations of the R1 and R1 FAC sheets, as well as to calculate the height-integrated Pedersen conductance (Σ_P) by assuming a simple linear relation between electric and magnetic field components.
2. The Σ_P values derived from the in situ observations follow the trend of the empirical Vickrey et al. (1981) model which is based only on the solar zenith angle. The Σ_P values under dark conditions have a spread of 0–10 S, in contrast to Σ_P values that are typically derived from solar zenith angle models (e.g., Fujii & Iijima, 1987; Haraguchi et al., 2004; Wang et al., 2005). However, these values are similar to those

reported by Brekke and Moen (1993) and Moen and Brekke (1993) in case studies of incoherent scatter radars data.

3. High level of correlation between the electric and magnetic fields during both sunlit and dark conditions suggests that the Σ_P values can remain uniform over large scales regardless of local time.
4. The upward FAC regions have larger data-derived Σ_P values than downward FAC regions in the dawn sector. This effect is not perceptible on the dusk side. Meanwhile, this effect is even more pronounced during the active substorm times for AE > 166 nT.
5. The previous point suggests that larger Σ_P in upward currents are likely caused by precipitating electrons, which can be more prominent during times of enhanced geomagnetic activity. Energetic electron precipitation in an upward FAC region can explain an increase in the ionospheric plasma density that would lead to enhanced Σ_P. These times are also commonly associated with observed pulsating and diffuse aurora (Kasahara et al., 2018) on the dawn side. However, the direct relation between elevated Pedersen conductance and aurora observations remains to be explored.

Data Availability Statement

The Swarm data can be obtained from the ESA server https://swarm-diss.eo.esa.int/. The release note for the TIICT 0301 cross-track ion drift data used in this study are available at https://earth.esa.int/documents/10174/1514862/Swarm-EFI-TII-Cross-track-flow-dataset-Release-Notes.pdf. The OMNI solar wind data and geomagnetic indices is available through the Coordinated Data Analysis Web (CDAWeb) server https://cdaweb.gsfc.nasa.gov/index.html/. The Supplementary materials for the paper are available at Zenodo archive https://doi.org/10.5281/zenodo.4779106.

Acknowledgments
The work would not have been possible without Canada-Norway mobility funds provided by the Norwegian Agency for International Cooperation and Quality Enhancement in Higher Education, project number NNA-2016/10081. JM and AS received funding from the Research Council of Norway grant 275653. JKB was supported in part by the Canadian Space Agency. Swarm is a European Space Agency (ESA) mission with major support from the Canadian Space Agency (CSA) for the EFI.

References

Akasofu, S.-I. (1968). Magnetospheric substorm. In *Polar and magnetospheric substorms* (pp. 212–253). Dordrecht: Springer Netherlands. https://doi.org/10.1007/978-94-010-3461-6_10

Birkeland, K. (1913). *The Norwegian aurora polaris expedition*. LeipzigBarth: Aschehoug.

Brekke, A., & Moen, J. (1993). Observations of high latitude ionospheric conductances. *Journal of Atmospheric and Terrestrial Physics*, *55*(11), 1493–1512. https://doi.org/10.1016/0021-9169(93)90126-J. (The XX IUGG General Assembly). Retrieved from http://www.sciencedirect.com/science/article/pii/002191699390126J

Burch, J. L., Reiff, P. H., Menietti, J. D., Heelis, R. A., Hanson, W. B., Shawhan, S. D., et al. (1985). IMF By -dependent plasma flow and Birkeland currents in the dayside magnetosphere: 1. Dynamics explorer observations. *Journal of Geophysical Research*, *90*(A2), 1577–1593. https://doi.org/10.1029/JA090iA02p01577

Duthie, D., & Scourfield, M. (1977). Aurorae and closed magnetic field lines. *Journal of Atmospheric and Terrestrial Physics*, *39*(11), 1429–1434. https://doi.org/10.1016/0021-9169(77)90099-X. Retrieved from http://www.sciencedirect.com/science/article/pii/002191697790099X

Erickson, G. M., Spiro, R. W., & Wolf, R. A. (1991). The physics of the harang discontinuity. *Journal of Geophysical Research*, *96*(A2), 1633–1645. https://doi.org/10.1029/90JA02344

Fang, X., Randall, C. E., Lummerzheim, D., Wang, W., Lu, G., Solomon, S. C., & Frahm, R. A. (2010). Parameterization of monoenergetic electron impact ionization. *Geophysical Research Letters*, *37*(22), L22106. https://doi.org/10.1029/2010GL045406

Feldstein, Y. I., Gromova, L. I., Woch, J., Sandahl, I., Blomberg, L., Marklund, G., & Meng, C.-I. (2001). Structure of the auroral precipitation region in the dawn sector: Relationship to convection reversal boundaries and field-aligned currents. *Annales Geophysicae*, *19*(5), 495–519. https://doi.org/10.5194/angeo-19-495-2001. Retrieved from https://hal.archives-ouvertes.fr/hal-00316842

Fremouw, E. J., Carlson, H. C., Potemra, T. A., Bythrow, P. F., Rino, C. L., Vickrey, J. F., et al. (1985). The HiLat satellite mission. *Radio Science*, *20*(3), 416–424. https://doi.org/10.1029/RS020i003p00416

Friis-Christensen, E., Lühr, H., Knudsen, D., & Haagmans, R. (2008). Swarm – An Earth observation mission investigating geospace. *Advances in Space Research*, *41*(1), 210–216. https://doi.org/10.1016/j.asr.2006.10.008. Retrieved from http://www.sciencedirect.com/science/article/pii/S0273117706005497

Fujii, R., & Iijima, T. (1987). Control of the ionospheric conductivities on large-scale Birkeland current intensities under geomagnetic quiet conditions. *Journal of Geophysical Research*, *92*(A5), 4505–4513. https://doi.org/10.1029/JA092iA05p04505

Fujii, R., Iijima, T., Potemra, T. A., & Sugiura, M. (1981). Seasonal dependence of large-scale Birkeland currents. *Geophysical Research Letters*, *8*(10), 1103–1106. https://doi.org/10.1029/GL008i010p01103

Greenwald, R. A., Shepherd, S. G., Sotirelis, T. S., Ruohoniemi, J. M., & Barnes, R. J. (2002). Dawn and dusk sector comparisons of small-scale irregularities, convection, and particle precipitation in the high-latitude ionosphere. *Journal of Geophysical Research*, *107*(A9). SIA 1-1–SIA 1-12. https://doi.org/10.1029/2001JA000158

Haraguchi, K., Kawano, H., Yumoto, K., Ohtani, S., Higuchi, T., & Ueno, G. (2004). Ionospheric conductivity dependence of dayside region-0, 1, and 2 field-aligned current systems: Statistical study with DMSP-F7. *Annales Geophysicae*, *22*(8), 2775–2783. https://doi.org/10.5194/angeo-22-2775-2004. Retrieved from https://hal.archives-ouvertes.fr/hal-00317563

Hardy, D. A., Gussenhoven, M. S., Raistrick, R., & McNeil, W. J. (1987). Statistical and functional representations of the pattern of auroral energy flux, number flux, and conductivity. *Journal of Geophysical Research*, *92*(A11), 12275. https://doi.org/10.1029/ja092ia11p12275

Iijima, T., & Potemra, T. A. (1976). The amplitude distribution of field-aligned currents at northern high latitudes observed by Triad. *Journal of Geophysical Research*, *81*(13), 2165–2174. https://doi.org/10.1029/JA081i013p02165

Jaynes, A. N., Lessard, M. R., Rodriguez, J. V., Donovan, E., Loto'aniu, T. M., & Rychert, K. (2013). Pulsating auroral electron flux modulations in the equatorial magnetosphere. *Journal of Geophysical Research: Space Physics*, *118*(8), 4884–4894. https://doi.org/10.1002/jgra.50434

Jaynes, A. N., Lessard, M. R., Takahashi, K., Ali, A. F., Malaspina, D. M., Michell, R. G., et al. (2015). Correlated pc4–5 ulf waves, whistler-mode chorus, and pulsating aurora observed by the Van Allen probes and ground-based systems. *Journal of Geophysical Research: Space Physics*, *120*(10), 8749–8761. https://doi.org/10.1002/2015JA021380

Jones, S. L., Lessard, M. R., Rychert, K., Spanswick, E., & Donovan, E. (2011). Large-scale aspects and temporal evolution of pulsating aurora. *Journal of Geophysical Research*, *116*(A3), A03214. https://doi.org/10.1029/2010JA015840

Kasahara, S., Miyoshi, Y., Yokota, S., Mitani, T., Kasahara, Y., Matsuda, S., et al. (2018). Pulsating aurora from electron scattering by chorus waves. *Nature*, *554*, 337–340. https://doi.org/10.1038/nature25505

King, J. H., & Papitashvii, N. E. (2005). Solar wind spatial scales in and comparisons of hourly wind and ace plasma and magnetic field data. *Journal of Geophysical Research*, *110*(A2), A02104. https://doi.org/10.1029/2004JA010649

Knudsen, D. J., Burchill, J. K., Buchert, S. C., Eriksson, A. I., Gill, R., Wahlund, J.-E., et al. (2017). Thermal ion imagers and Langmuir probes in the Swarm electric field instruments. *Journal of Geophysical Research: Space Physics*, *122*(2), 2655–2673. https://doi.org/10.1002/2016JA022571

Knudsen, D. J., Kelley, M. C., Earle, G. D., Vickrey, J. F., & Boehm, M. (1990). Distinguishing Alfvén waves from quasi-static field structures associated with the discrete aurora: Sounding rocket and HILAT satellite measurements. *Geophysical Research Letters*, *17*(7), 921–924. https://doi.org/10.1029/GL017i007p00921

Knudsen, D. J., Kelley, M. C., & Vickrey, J. F. (1992). Alfven waves in the auroral ionosphere: A numerical model compared with measurements. *Journal of Geophysical Research*, *97*(A1), 77. https://doi.org/10.1029/91ja02300

Korth, H., Zhang, Y., Anderson, B. J., Sotirelis, T., & Waters, C. L. (2014). Statistical relationship between large-scale upward field-aligned currents and electron precipitation. *Journal of Geophysical Research: Space Physics*, *119*(8), 6715–6731. https://doi.org/10.1002/2014JA019961

Koustov, A. V., Lavoie, D. B., Kouznetsov, A. F., Burchill, J. K., Knudsen, D. J., & Fiori, R. (2019). A comparison of cross-track ion drift measured by the Swarm satellites and plasma convection velocity measured by SuperDARN. *Journal of Geophysical Research: Space Physics*, *124*(6), 4710–4724. https://doi.org/10.1029/2018JA026245

Li, W., Bortnik, J., Thorne, R. M., & Angelopoulos, V. (2011). Global distribution of wave amplitudes and wave normal angles of chorus waves using THEMIS wave observations. *Journal of Geophysical Research:*, *116*(A12), A12205. https://doi.org/10.1029/2011JA017035

Lomidze, L., Burchill, J. K., Knudsen, D. J., Kouznetsov, A., & Weimer, D. R. (2019). Validity study of the Swarm horizontal cross-track ion drift velocities in the high-latitude ionosphere. *Earth and Space Science*, *6*(3), 411–432. https://doi.org/10.1029/2018EA000546

Lummerzheim, D., & Lilensten, J. (1994). Electron transport and energy degradation in the ionosphere: Evaluation of the numerical solution, comparison with laboratory experiments and auroral observations. *Annales Geophysicae*, *12*(10), 1039–1051. https://doi.org/10.1007/s00585-994-1039-7

Lyatsky, S., Khazanov, G., & Zesta, E. (2014). Interhemispheric field-aligned currents: Simulation results. *Journal of Geophysical Research: Space Physics*, *119*, 5600–5612. https://doi.org/10.1002/2013JA019558

Lyons, L. R., & Fennell, J. F. (1986). Characteristics of auroral electron precipitation on the morningside. *Journal of Geophysical Research*, *91*(A10), 11225–11234. https://doi.org/10.1029/JA091iA10p11225

Lysak, R. L. (1985). Auroral electrodynamics with current and voltage generators. *Journal of Geophysical Research*, *90*(A5), 4178–4190. https://doi.org/10.1029/JA090iA05p04178

Marsal, S. (2015). Conductivities consistent with Birkeland currents in the AMPERE-driven TIE-GCM. *Journal of Geophysical Research: Space Physics*, *120*(9), 8045–8065. https://doi.org/10.1002/2015JA021385

McGranaghan, R., Knipp, D. J., Matsuo, T., & Cousins, E. (2016). Optimal interpolation analysis of high-latitude ionospheric Hall and Pedersen conductivities: Application to assimilative ionospheric electrodynamics reconstruction. *Journal of Geophysical Research: Space Physics*, *121*(5), 4898–4923. https://doi.org/10.1002/2016JA022486

McGranaghan, R., Knipp, D. J., Matsuo, T., Godinez, H., Redmon, R. J., Solomon, S. C., & Morley, S. K. (2015). Modes of high-latitude auroral conductance variability derived from DMSP energetic electron precipitation observations: Empirical orthogonal function analysis. *Journal of Geophysical Research: Space Physics*, *120*(12), 11013–11031. https://doi.org/10.1002/2015JA021828

Moen, J., & Brekke, A. (1993). The solar flux influence on quiet time conductances in the auroral ionosphere. *Geophysical Research Letters*, *20*(10), 971–974. https://doi.org/10.1029/92GL02109

Newell, P. T., Meng, C.-I., & Lyons, K. M. (1996). Suppression of discrete aurorae by sunlight. *Nature*, *381*(6585), 766–767. https://doi.org/10.1038/381766a0

Nishimura, Y., Bortnik, J., Li, W., Thorne, R. M., Chen, L., Lyons, L. R., et al. (2011). Multievent study of the correlation between pulsating aurora and whistler mode chorus emissions. *Journal of Geophysical Research*, *116*(A11), A11221. https://doi.org/10.1029/2011JA016876

Nishimura, Y., Bortnik, J., Li, W., Thorne, R. M., Lyons, L. R., Angelopoulos, V., et al. (2010). Identifying the driver of pulsating aurora. *Science*, *330*(6000), 81–84. https://doi.org/10.1126/science.1193186. Retrieved from https://science.sciencemag.org/content/330/6000/81

Pakhotin, I. P., Mann, I. R., Lysak, R. L., Knudsen, D. J., Gjerloev, J. W., Rae, I. J., et al. (2018). Diagnosing the role of Alfvén waves in magnetosphere-ionosphere coupling: Swarm observations of large amplitude nonstationary magnetic perturbations during an interval of northward IMF. *Journal of Geophysical Research: Space Physics*, *123*(1), 326–340. https://doi.org/10.1002/2017JA024713

Palmroth, M., Janhunen, P., Pulkkinen, T. I., Aksnes, A., Lu, G., Østgaard, N., et al. (2005). Assessment of ionospheric joule heating by GUMICS-4 MHD simulation, AMIE, and satellite-based statistics: Towards a synthesis. *Annales Geophysicae*, *23*(6), 2051–2068. https://doi.org/10.5194/angeo-23-2051-2005. Retrieved from https://www.ann-geophys.net/23/2051/2005/

Rich, F. J., Hardy, D. D., & Gussenhoven, M. S. (1985). Enhanced ionosphere-magnetosphere data from the DMSP satellites. *Eos, Transactions American Geophysical Union*, *66*(26), 513–514. https://doi.org/10.1029/EO066i026p00513

Robinson, R. M., Vondrak, R. R., Miller, K., Dabbs, T., & Hardy, D. (1987). On calculating ionospheric conductances from the flux and energy of precipitating electrons. *Journal of Geophysical Research*, *92*(A3), 2565–2569. https://doi.org/10.1029/JA092iA03p02565

Sugiura, M., Maynard, N., Farthing, W., Heppner, J., Ledley, B., & Cahill, L., Jr. (1982). Initial results on the correlation between the magnetic and electric fields observed from the DE-2 satellite in the field-aligned current regions. *Geophysical Research Letters*, *9*(9), 985–988. https://doi.org/10.1029/GL009i009p00985

Thébault, E., Finlay, C. C., Alken, P., Beggan, C. D., Canet, E., Chulliat, A., et al. (2015). Evaluation of candidate geomagnetic field models for IGRF-12. *Earth Planets and Space*, *67*(1), 112. https://doi.org/10.1186/s40623-015-0273-4

Thorne, R. M., Ni, B., Tao, X., Horne, R. B., & Meredith, N. P. (2010). Scattering by chorus waves as the dominant cause of diffuse auroral precipitation. *Nature*, *467*, 943–946. https://doi.org/10.1038/nature09467

Vickrey, J. F., Vondrak, R. R., & Matthews, S. J. (1981). The diurnal and latitudinal variation of auroral zone ionospheric conductivity. *Journal of Geophysical Research*, *86*(A1), 65–75. https://doi.org/10.1029/JA086iA01p00065

Wang, H., Lühr, H., & Ma, S. Y. (2005). Solar zenith angle and merging electric field control of field-aligned currents: A statistical study of the southern hemisphere. *Journal of Geophysical Research*, *110*(A3), A03306. https://doi.org/10.1029/2004JA010530

Watanabe, M., Iijima, T., Nakagawa, M., Potemra, T. A., Zanetti, L. J., Ohtani, S.-I., & Newell, P. T. (1998). Field-aligned current systems in the magnetospheric ground state. *Journal of Geophysical Research*, *103*(A4), 6853–6869. https://doi.org/10.1029/97JA03086